The Role of Groundbased Radar in Near-Earth-Object Hazard Identification and Mitigation

Steven J. Ostro

300-233, Jet Propulsion Laboratory
California Institute of Technology
Pasadena, CA 91109-8099

(818) 354-3173, fax -9476
ostro@echo.jpl.nasa,gov

A chapter for *Hazards Due to Comets and Asteroids*,
T. Gehrels and M. S. Matthews, eds.
University of Arizona Press, Tucson

Abstract

Groundbased radar is a key technique for the post-discovery reconnaissance of NEOS and is likely to play a central role in identification of possibly threatening objects during the foreseeable future. Delay-Doppler measurements are orthogonal to optical angle measurements and typically have a fractional precision between 10^{-5} and 10^{-9}, and consequently are invaluable for refining orbits and prediction ephemerides. The same measurements can provide two-dimensional images with resolution on the order of decimeters. Imaging data sets with adequate coverage in subradar longitude/latitude can be used to determine the target's shape and spin vector. The active planetary radars use wavelengths that are sensitive to near-surface bulk density and structural scales larger than a few centimeters and, for comets, can penetrate optically opaque comas and reveal large-particle clouds. Upgrades of existing telescopes (especially Arecibo) will expand the range of groundbased radar and will optimize NEO imaging and astrometric capabilities. However, existing instruments are already oversubscribed, and observation of more than a small fraction of objects discovered in a Spaceguard-like survey will require radar telescopes dedicated to NEO reconnaissance.

1. INTRODUCTION

The goal of this chapter is to assess the, potential role of groundbased radar in confrontation of the NEO hazard now and in the future. The next section is a tutorial in current NEO radar techniques, with emphasis on measurements useful for orbit refinement and physical. characterization. The state of NEO radar reconnaissance is described in Section III, which briefly summarizes pre-1993 observations and discusses expectations for NEO work after 1994, when telescope upgrades" now underway should be finished. Section IV offers scenarios for radar involvement in NEO threat assessment during the Spaceguard era and some speculations on possible developments during the next millennium.

Any discussion of the NEO hazard requires "boundary conditions" that define the domain of that discussion. In this chapter, the term "impact hazard" is meant to have a very broad connotation. In particular, 1 consider a prediction of an impact to be potentially hazardous, because it might provoke

an economically or psychologically destructive societal response, even if the predicted collision were known to be insufficiently energetic to affect the global ecology. Moreover, under certain circumstances such a prediction could lead to development of a mitigation system whose existence would in itself introduce a significant risk to civilization (Sagan and Ostro, 1993) .

An underlying reality of the asteroid/comet hazard is that there will be a progression from dedicated search programs (e.g., the proposed Spaceguard Survey; see Morrison, 1992) to identification of objects that might threaten collision within some time interval (e.g., the next century), to progressive refinement of each threat assessment, eventually resulting in classification of the object as nonthreatening or in decisions to take increasingly serious forms of action, beginning with spacecraft reconnaissance and proceeding to defensive operations, until we no longer believe there to be any danger. The overriding considerations throughout t-his entire process will be the state of our uncertainty about threatening objects and their trajectories, what can be done to reduce that uncertainty, and the cost of doing so. One can, in fact., view civilization's response to the NEO hazard as involving three stages of ignorance . First, and most fundamentally, although we know the gross character of the population and average collision rates, we have identified only an insignificant fraction of the potential impactors. The Spaceguard Survey is intended to be the initial. step toward dispelling this kind of ignorance. The second kind of uncertainty concerns known objects' orbits and the circumstances of future close approaches. The third kind of uncertainty concerns the outcome of the impact of a specific object on a specific collision course, and hence the object's physical properties, including mass, dimensions, composition, internal structure, and multiplicity. If spacecraft inspection or defensive action are to be undertaken, then spin state, detailed surface properties, and the presence of accompanying swarms of macroscopic particles would be relevant as well . Groundbased radar is uniquely suited for cost--effective trajectory refinement and physical characterization. As will become clear in the text that follows, these two roles are inseparable in practice.

II. CURRENT NEO RADAR TECHNIQUES

The general stratagem of a radar observation is to transmit an intense, coherent signal with very well-known polarization state and time/frequency structure and then, by comparing those properties to the measured properties of the echo, deduce the properties of the target. The information content of an observations will depend on the echo strength, which must be at least several times greater than the rms fluctuation in the receiver's thermal noise. The signal-to-noise ratio is proportional to factors describing the radar system and the target:

$$\text{SNR} \sim (\text{SYSTEM FACTOR})\ (\text{TARGET FACTOR})\ (\Delta t)^{1/2} \tag{1}$$

where

$$\text{SYSTEM FACTOR} \sim P_{tx}\, A_{tx}\, \eta_{rec} / \lambda^{3/2}\, T_{sys}$$

$$\sim P_{tx}\, G_{tx}\, \eta_{rec}\, \lambda^{5/2} / T_{sys} \tag{2}$$

and

$$\text{TARGET FACTOR} \sim \hat{\sigma}\, D^{3/2}\, P^{1/2} / R^4 \tag{3}$$

Here At is integration time, P_{tx} is transmitted power, λ is wavelength, and T_{sys} is the system temperature. A_{tx} and A_{rcv} are effective (i.e., illuminated) antenna apertures during transmit and receive, and are related to the corresponding antenna gains G_{tx} and G_{rcv} by $G/4\pi = A/\lambda^2$. In Eq. (3), the target properties are effective diameter D, spin period P, distance R, and radar albedo $\hat{\sigma}$, which is the ratio of radar cross section σ to projected area $\pi D^2/4$.

Telescopes

The two continuously active planetary radar telescopes are the Arecibo (λ = 13 and 70 cm) and GoldsLone (3.5 and 13 cm) instruments. For each, the shorter wavelength provides much greater sensitivity and is the exclusive choice for NEO work, and representative values of optimum system characteristics are P_{tx} -- 450 kW, gain - $10^{7.1}$, and T_{sys} - 25 K. The Arecibo 13-cm (S-band, 2380-MHz) system has for the past five years been twice as

sensitive as the Goldstone 3.5-cm (X-band, 8510-MHZ) system, but Goldstone can track targets continuously for much longer periods and has access to the whole sky north of -40° declination. Two bistatic (two-station) experiments have been carried out at Goldstone, first with 1566 Icarus in 1968 and most recently with 4179 Toutatis in 1992. The latter used transmission from the 70-m antenna (DSS 14) and reception 21 km away with a new 34-m beam-waveguide antenna (DSS 13). Toutatis also was the target of a Russi.an-German bistatic experiment (the first non-U.S. asteroid radar observations), which used transmission from the Yevpatoria 100-m antenna in Crimea and reception from the Effelsberg 100-m antenna near Bonn, Germany (Zaytsev et al., 1993). Aperture-synthesis observations, employing 3.5-cm transmission from Goldstone and reception of echoes at the 27-antenna Very Large Array (VLA) in New Mexico, have been carried out for two NEOs, 1991 EE and Toutatis (de Pater et al., 1992, 1993). That system can synthesize a beamwidth as small as 0.25 seconds of arc, vs. 2 minutes of arc for single-dish observations.

The Goldstone 14/13 system and the Yevpatoria/Effel.sberg 6-cm system are, respectively, about 50% and 30% as sensitive as the Goldstone monostatic (DSS-14) system. The Goldstone-VLA system is three times as sensitive as the Goldstone monostatic system, but only for targets with bandwidths no less than 381 Hz; for narrower echoes, including those from NEOs, the SNR falls off in proportion to the square root of the echo bandwidth.

The Arecibo telescope is being upgraded to increase its sensitivity by more than an order of magnitude by constructing a ground screen around the periphery of the dish, replacing high-frequency line feeds with a Gregorian subreflector configuration, doubling the transmitter power, and installing a fine-guidance pointing system. At Goldstone, installation of a new transmit-receive feed horn and a new data-acquisition system will optimize observations of close NEOs.

Figure 1 shows the relative sensitivities of the primary planetary radar systems as a function of target declination. Arecibo will have twice the range and will see three times the volume of Goldstone, while Goldstone will see twice the plane-of-sky solid angle and will have three times the hour angle coverage of Arecibo.

The value of a radar observation increases in proportion to the echo strength. An SNR as large as 20 is usually adequate for detection and marginal resolution of the echoes. SNRS greater than 100 let one achieve enough resolution to be able to make simple statements about shape. With SNRs ~ 1000, the data permit detailed constraints on size and shape, and with SNRS approaching 10,000 one can make images that clearly show surface features. Very crudely, one can expect the number of useful (low-noise) pixels in a dataset to be of the same order as the SNR.

Disc-Integrated Measurements

In most modern radar observations, the transmission is circularly polarized and two parallel receiving channels are used to receive echoes in the same circular polarization as transmitted (the SC sense) and simultaneously in the opposite (OC) sense. The handedness, or helicity, of a circularly polarized wave is reversed on normal reflection from a plane mirror, so single backreflections from dielectric interfaces whose sizes and radii of curvature greatly exceed the wavelength yield echoes almost entirely in the OC polarization. SC echo power can arise from multiple scattering, from single backscattering from interfaces with wavelength-scale radii of curvature (e.g., rocks), or from subsurface refraction. Therefore the circular polarization ratio

$$\mu_C = \sigma_{SC}/\sigma_{OC} \tag{4}$$

is a useful gauge of the target's near-surface, wavelength-scale complexity, or "roughness". When linear polarizations are used, it is convenient to define the linear polarization ratio

$$\mu_L = \sigma_{SL}/\sigma_{OL}. \tag{5}$$

Both μ_L and μ_C would be zero for a perfectly smooth target. For all NEO radar measurements to date, $\mu_L < 1$ and $\mu_L < \mu_C$.

Widely used measures of radar reflectivity are the OC radar albedo

$$\hat{\sigma}_{OC} = \sigma_{OC}/A_{proj}, \tag{6}$$

where A_{proj} is the target's projected area, and the total power (OC + SC = OL + SL) radar albedo $\hat{\sigma}_T$, which is four times the geometric albedo used in optical planetary astronomy. A smooth metallic sphere would have $\hat{\sigma}_{OC} = \hat{\sigma}_{SL} = 1$.

For solid-surfaced targets with low μ_C, the physical interpretation of the radar albedo is clear-cut, as the surface must be smooth at all scales within about an order of magnitude of the wavelength and the subsurface must lack structure at those scales down to several 1/e power absorption lengths L. Here we may interpret the radar albedo as the product $g\rho$, where p is the Fresnel power reflection coefficient at normal incidence and the backscatter gain g depends on target orientation, shape, and the distribution of surface slopes with respect to that shape. Large mainbelt objects are expected to be covered with regoliths more than 15 m thick; in light of expectations about such objects' shapes and surface slope distributions, g is probably within a few tens of percent of unity, so $\hat{\sigma}_{OC}$ is a reasonable first approximation to p (Ostro et al., 1985). For the smaller, more irregularly shaped NEAs, g might be a strong function of orientation, causing radar cross section to vary much more dramatically than A_{proj} as the object rotates. NEO albedos derived from observations with thorough rotation phase coverage might tend to "average out" variations in g, but possibly not enough to justify treating $\hat{\sigma}_{OC}$ as an approximation to p.

Both p and I, depend on interesting characteristics of the surface material, including bulk density, porosity, particle size distribution, and metal abundance (see, e.g., Ostro et. al. 1991a and references therein). For example, L is several wavelengths for solid assemblages (rocks) of common silicate minerals and is of order ten wavelengths for powdered assemblages with porosities -45%, a typical value for the lunar regolith. Corresponding values for water ice are orders of magnitude larger. For dry, unconsolidated powders of meteoritic minerals, p depends primarily on bulk density d, and predictions of p(d) based on empirical functions probably are reliable to -25%. For solids, small volume concentrations V of metal particles in a silicate matrix can raise p above the value for $V = 0$ by an amount that depends on the electrical properties of each phase, the metal particles' dimensions and packing geometry, and V. Predictions of the rather large ranges of p for

several meteorite types on the basis of laboratory investigations of "loaded dielectrics" are consistent with available measurements of P for meteorite specimens. Solids are more reflective than powders, so inferences of metal concentration and meteoritical association from radar albedos necessarily involve assumptions about regolith depth and porosity. 'I'he radar absorption length in dry, powdered rocks is about 10 wavelengths, so a regolith more than one meter thick would hide underlying bedrock from the radar. A much thinner regolith can act similarly if it has a density gradient that. matches the bedrock's impedance to that of free space, or if it has stratifications containing 10SSY layers that create certain resonance effects.

If $\mu_C >> 0.1$, then physical interpretations are rarely very unique, because models must consider not just the nature of the surface/space interface but also the regolith's structural and electrical properties, including the size distribution, spatial. di.stribution, and scattering properties of subsurface rocks. One modeling complication is that multiply scattered radiation includes a diffusely scattered part as well as a coherent backscattered peak due to constructive interference between waves traveling on geometrically identical. but time-reversed paths (Mishchenko 1992) .

Time delay and Doppler frequency

In monostatic experiments transmit/receive cycles, or runs, consist of transmission for a duration close to the signal's roundtrip time delay (until the first echoes are about to come back), followed by reception of echoes for a similar duration. A bistatic configuration obviates this transmit/receive cycling.

In continuous wave (cw) observations, one transmits an unmodulated, nearly monochromatic waveform and measures the distribution of echo power as a function of frequency. In ranging observations, modulation of the waveform permits measurement of the distribution of echo power in time delay as well. The echo time delay and Doppler frequency shift change continuously due to the relative motion of the target with respect to the radar. To avoid smearing of accumulated echoes in time and frequency, one tunes the receiver's front-end local oscillator according to an ephemeris based on an *a priori* orbit. Sometimes it is more convenient to take out the Doppler on the uplink, that is, to continuously tune the transmitter so the receiver sees a constant. carrier

frequency. In time-resolved experiments, one drifts the sampling time base according to the predicted rate of change of time delay to maintain constant registration of the samples with respect. to the target's center of mass.

Time and frequency measurements have paramount importance in NEO radar astronomy, because the Lime-delay/Doppler-frequency distribution of echo power is the source of fine spatial resolution, and also because delay and Doppler are fundamental dynamical observable. In simple terms, the roundtrip time delay, τ, between transmission of a signal and reception of its echo is approximately $2R/c$, with c the speed of light and R the distance to the target. The time delay is 998 seconds for a target 1 AU from the radar, 2.5 seconds for the Moon, and typically between a few tens of seconds and a few minutes for NEOS observed so far. The echo's Doppler frequency v is approximately $2F_{tx}v_{rad}/c$, where F_{tx} is the transmitter carrier frequency and v_{rad} is the target's radial velocity; thus the magnitude of v in hertz is simply the radial velocity in half wavelengths per second.

Different parts of a rotating target have different velocities relative to the radar, so the echo will be dispersed in Doppler as well as in delay. The dispersion and the detailed functional form of the delay-Doppler distribution of echo power, $\sigma(\tau,\nu)$, depends on the target's size, shape, scattering characteristics, and orientation. For a sphere with diameter D and apparent. rotation period P, echoes would have a delay depth $\Delta\tau_{TARGET} = D/c$ and a bandwidth $\Delta\nu_{TARGET} = (4\pi D \cos\delta)/\lambda P$, where δ is the angle between the radar line of sight and the target's equatorial 'plane. Radar experiments aim to constrain the target's properties by measuring $\sigma(\tau,\nu)$, perhaps with more than one combination of transmitted and received polarizations and perhaps as a function of time, i.e., as a function of the target's orientation and direction. Ideally, one would like to obtain $\sigma(\tau,\nu)$ with very fine resolution, sampling that function within cells whose dimensions, $\Delta\tau$ x Av, are small compared to the echo dispersions (to achieve fine fractional resolution of the echoes) and as small as possible compared to the magnitudes of the echo's mean delay and Doppler (to permit refinement of the target's orbit).

Waveforms and Signal Processing

In cw experiments, complex voltage samples of the received signal are Fourier transformed and the resultant real and imaginary components are squared

and summed to obtain an estimate of the power spectrum; the frequency resolution equals to the reciprocal of the time series' length, i.e., of the coherence time. The number of fast Fourier transforms (FFT's) applied to data from a single transmit/receive cycle can range from one to tens of thousands. All NEOs are sufficiently narrowband for power spectra to be computed and accumulated in an array processor and recorded directly on magnetic tape at convenient intervals, but often it is preferable to record voltages for post-real-time Fourier analysis, perhaps using FFTs of different lengths to obtain spectra at various frequency resolutions.

Delay resolution requires a modulated waveform. For example, with a coherent-pulsed-cw waveform, the transmitt.er's carrier-frequency oscillator operates continuously but power is radiated only during intervals that are one delay resolution cell long and occur at intervals called the pulse repetition period (PRP), which should exceed the target's delay depth to ensure that the echo will consist of successive, nonoverlapping range profiles. The reciprocal of the PRP is the maximum effective sampling rate at any given delay. Fourier transformation of N samples of the signal's complex voltage taken at the same position within each of N successive range profiles (that is, the same delay relative to the delay of hypothetical echoes from the target's center of mass) yields the echo spectrum for the corresponding range cell on the target, with a frequency resolution B/N. The bandwidth, and hence the recording rate and the spectral resolution achievable with a given FFT length, can be reduced by a factor of N_{coh} in real time by coherently summing N_{coh} successive, PRP-long time series of voltage samples.

Almost all NEO radar ranging has used a binary phase-coded cw waveform to simulate a coherent pulsed-cw waveform. The basic time interval of the phase-coded waveform, called the baud, sets the delay resolution At. Once every At seconds, the phase of the transmitted signal is either shifted by 180° or not, according to the value of the corresponding element in binary code. Shift-register, "pseudo-random" binary codes, which are easy to generate and have very sharply peaked autocorrelation functions, are ubiquitous in radar astronomy. Shi.ft-register code lengths equal 2M -1, with M a whole number. In most. delay/Doppler experiments the code is repeated continuously during the transmission, so the PRP is the product of the baud and the code length. The

received signal is decoded by Cross-correlating it. with a replica of a single code cycle.

Current planetary radars work with waveforms that provide time resolution as fine as 10 μs. This limit, set by the 10-MHZ modulation bandwidth of klystron amplifiers, corresponds to 15-m range resolution. Bounds on the frequency resolution $\Delta\nu$ are set primarily by the reciprocal of coherence times of recordable data sets; in monostatic experiments, $\Delta\nu \geq 1/\mathrm{RTT}$.

Ephemerides and Delay-Doppler Astrometry

A singularly important aspect of NEO radar astronomy is the precision and reliability of time/frequency measurements that are made possible by high-speed data acquisition systems and stable, accurate clocks and frequency standards (e.g., Seidelmann et al., 1992) . This fine measurement precision places stringent demands on the accuracy of NEO ephemerides, because the predictions of delay and Doppler [$\tau_{eph}(t)$ and $\nu_{eph}(t)$] must be accurate enough to prevent smearing of echoes, which would compromise the data's SNR and delay/Doppler resolution. For example, since

$$d\tau(t)/dt = -v(t)/F_{tx}, \tag{7}$$

a Doppler prediction error of $\Delta\nu_{eph}$ will cause echoes integrated over one roundtrip time RTT to be smeared in time delay by $(-\Delta\nu_{eph}/F_{tx})\mathrm{RTT}$. For new NEOS, errors in prediction ephemerides are very large and grow rapidly, because orbits must be estimated from optical astrometric data that span very short arcs. During initial radar observations of such an object at 0.04 AU (RTT ~ 40 s) the delay uncertainty might be 0.4 s (~10 Earth radii) and the 2380-MHz Doppler uncertainty might be 1 kHz (or 17ms of delay smear in a 40-sreceive period) . A delay measurement with a 40-μs baud could reduce the instantaneous delay uncertainty by four orders of magnitude, allowing one to generate more accurate delay-Doppler predictions, which would permit much more precise radar astrometry, and so on. This iterative, "bootstrapping" process has long characterized both the radar improvement of orbits and the refinement of the models and computational techniques that are the basis of the planetary ephernerides(e.g., Standish et al ., 1992) .

Current needs of NEO radar astronomy are served by the programs PEP770 at_ the Harvard-Smithsonian Center for Astrophysics and DE200 at the Jet Propulsion

Laboratory. Prior to the advent of electronic networks, ephemerides were transported by magnetic tape. Nowadays, ephemerides are sent over the Internet and it is not uncommon for an NEO track on any given day to use an ephemeris based on all radar and optical astrometry reported through the previous day. In the near future, computation of updated ephemerides will be possible with on-site computers, permitting near-real-time bootstrapping of new generations of ephemerides from delay-Doppler measurements as soon as they are made. With such a system, it will be possible to progress from an initial detection to high-resolution imaging within one several-hour track.

Most available NEO radar astrometry consists of an estimate of $\tau(t)$ or $\nu(t)$ for echoes received at the telescope's reference point at a specified UTC epoch t. For example, Arecibo observations are referenced to the center of curvature of the main reflector. The Earth-fixed coordinates of these points are tabulated by Yeomans et al. (1992) . Usually it is adequate to think of the offsets $[-to(t) = T(t) - \tau_{eph}(t)$ and $\nu_o(t) = \nu(t) - \nu_{eph}(t)]$ of the echoes from the ephemeris predictions as being constant over the pertinent measurement time scales, typically from one roundtrip time to a few hours. In practice, one measures τ_o or ν_o and reports $\tau(t)$ or $\nu(t)$ for a convenient epoch near the weighted mean time of the measurements.

Radar astrometry during the discovery apparition can ensure optical recovery of newly discovered NEOs, because delay-Doppler measurements have fine fractional precision and are orthogonal to optical, angular-position measurements (Yeomans et al., 1987) . As discussed in Yeomans' chapter, radar astrometry commonly improves upon the accuracy of optical-only ephemerides of newly discovered NEAs by one to three orders of magnitude. Even for asteroids with very long astrometric histories and secure orbits, radar measurements can significantly shrink positional. error ellipsoids for decades, with direct implications for the navigation of spacecraft to asteroids and predictions of extremely close approaches of asteroids to Earth.

Delay-Doppler Imaging

Radar can image NEOS if the echoes are strong enough. Continuous wave (cw) observations yield echo spectra, $\sigma(\nu)$, that can be thought of as one-dimensional images, or brightness scans across the target through a slit parallel to the asteroid's apparent (synodic) spin vector. As discussed by

Ostro et al. (1988), the bandwidth of a target's instantaneous echo power spectrum is proportional to the breadth, measured normal to the line of sight., of the target's pole-on silhouette, and measurements of echo edge frequencies as functions of rotation phase can be used to estimate the shape (and the size in units of km/cos δ) of the convex envelope, or hull, of the silhouette as well as the frequency of hypothetical echoes from the asteroid's center of mass (COM) .

Time-modulated waveforms yield a range profile $\sigma(\tau)$ and in most cases a delay-Doppler image $\sigma(\tau,\nu)$. The point on the surface with the shortest echo time delay is called the subradar point. Parallax effects and the curvature of the incident wave front are negligible for groundbased radar observations, so contours of constant delay are intersections of the target's surface with planes perpendicular to the line of sight. Constant-Doppler planes are parallel to the line of sight and al-so parallel to the target's synodic spin vector. Thus one can imagine two orthogonal sets of parallel planes that cut the target into delay-Doppler cells like one dices a potato to make french fries . For a spherical target viewed equatorially, each bin of the dicer that contains the equator will define one surface cell, while each bin that is too close to the spin vector to contain the equator will define one surface cell in the northern hemisphere and one in the southern hemisphere. That is, for most of the sphere there is a two-to-one mapping from surface coordinates to delay-Doppler coordinates, so a delay-Doppler image is north/south ambiguous. For an equatorial view, any pair of N/S ambiguous points have longitudes that are identical and latitudes that have the same magnitude but opposite signs, i.e., the two points are symmetrically located with respect to the target's equatorial plane. These points would execute identical delay-Doppler trajectories as the target rotates. However, if the subradar latitude were nonzero, two points at any given longitude and opposite latitudes would execute different delay-Doppler trajectories as a function of rotation phase ϕ, so one could invert delay-Doppler images taken at a variety of phases to overcome the N/S ambiguity. If the shape of the target were known *a priori*, one could solve for the global distribution of albedo (Hudson and Ostro 1990); this approach may be suitable for the largest mainbelt asteroids. For NEOs, shape is the fundamental unknown, so the inversion would, at. least at first, assume homogeneous scattering properties and try to solve for the shape (Hudson 1992, 1993) . Such an inversion would also model the spin vector and the delay-

Doppler trajectory of the target's center of mass, and hence would involve a rather complex parameter space. The estimation accuracy for the various parameters will depend on the geometrical leverage of the data (i.e., the subradar longitude/latitude coverage, the data's SNR and fractional delay-Doppler resolution, and of course the target's physical configuration. For example, images of a very flat object viewed off the equator would have no N/s ambiguities, whereas images of a highly nonconvex, multi-component target conceivably could have four-fold ambiguities.

Several other attributes of radar images deserve mention. First, whereas optical images are projections of brightness onto a plane normal to the line of sight, a delay-Doppler image is the projection of the target's radar brightness onto a plane containing the radar and hence parallel to the line of sight. Second, the term "radar image" usually refers to a measured distribution of echo power in delay, Doppler, and/or angular coordinates, while term "radar map" usually refers to a display in target-centered coordinates of the residuals with respect to a model that parameterizes the target's average scattering properties. Third, radar images are time exposures, because the frequency resolution is the reciprocal of the integration time of complex voltage samples coherently processed into 'a single power spectrum (one look) , and the fractional self-noise in an incoherent sum of N looks is $N^{-1/2}$. Hence there is a trade-off between spatial resolution, self-noise, and motion-induced smearing. [This topic is discussed by Stacy (1993) in the context of high-resolution radar imaging of the Moon.]

If an imaging dataset has thorough subradar longitude coverage and also samples northern and southern middle latitudes, then the target's shape, center of mass location, and spin vector might be so well constrained that information about. the target's internal. density distribution might also be derivable.

III. THE CURRENTSTATEOF NEORADAR RECONNAISSANCE

Summary of Investigations Through 1992

Table I lists radar-detected comets and near--Earth asteroids. Papers reporting focused analyses for specific targets are cited in that table. Pre-1991 NEO radar astrometry is present.ed by Ostro, Campbell, Chandler, et. al.

(1991b) . Yeomans et al. (1992) outline "techniques required to use delay-Doppler measurements in orbit estimations and give orbits for 34 targets based on the combined radar and optical data. As an example of recent radar astrometry, observations of 1991 JX with a 0.2-microsecond baud yielded a time-delay estimate whose fractional precision is 5×10^{-9}. Table 11 shows how radar astrometry during that object's discovery apparition yields a 300-fold improvement over optical-only prediction of that object's location decades after discovery. The most precise NEO delay/Doppler measurements to date were obtained for Toutatis in 1992: a 0.125-μs time–delay measurement with a fractional precision of 2×10^{-9} and a 0.0083-Hz Doppler measurement at F_{TX} = 8510 MHz (equivalent to v_{rad} = 150 ~/see) with a fractional precision of 2×10^{-8}. During the past decade, observations of newly discovered objects have revealed range errors from ~100 km to -100, OOO km in pre-radar ephemerides (Fig. 2).

Radar cross sections and circular polarization ratios for most of the radar-detected NEAs were reported by Ostro et al. 1991) . Figure 3 plots values of $\hat{\sigma}_{OC}$ vs. μ_C for several NEAs; there clearly is a great deal of diversity evident even in these objects' disc-integrated radar properties. In terms of imaging, the two most productive experiments so far were the observati.ons of 4769 Castalia in 1989 and of 4179 Toutatis in 1992. The key Castalia images were taken in a 2.5–h period, cover -240° of rotation phase at a nonzero subradar latitude, and consist of 64 frames, each of which was constructed from 26 looks and places a few dozen pixels on the target. The data are adequate to define the shape at a scale ~ 100 m, or ~5% of the object's maximum overall dimension, as well as the spin period and the subradar latitude (Hudson and Ostro, 1993). The Toutatis imaging experiment spanned 2.5 weeks and -125° of geocentric direction, but no more than two synodic rotations. The most useful images place more than 1000 pixels on the target. However, because the resolution is so fine, rotational motion and ephemeris drift are evident over times comparable to an interval containing enough looks to shrink the self-noise to a comfortable level.. Hence, extraction of the full information contained in those images must rely on a model that parameterizes the surface in fine detail (to scales ~ 10 m) .

Both Castalia and Toutatis are strongly bifurcated objects. Very coarse-resolution images of 1627 Ivar and 1986 DA, as well as echo spectra for 2201 Oljato and 3908 (1980 PA) show clearly bimodal distributions of echo power. Thus some 20% of the NEA radar sample shows at least some indication of double-lobed structure; for another 20% of the sample the SNR was too low for useful spatial resolution. On Earth, three out, of the 28 known impact craters with diameters > 20 km are doublets. Melosh and Stansberry (1991) analyzed the occurrence of widely separated doublet craters on Earth and suggested that some 10% of the estimated -2000 kilometer-sized ECAs may be well separated binary asteroids. "Double" objects may therefore be fairly common in the NEA population. Of course, it would be highly desirable to know an object's gross physical configuration prior to spaceborne reconnaissance.

Cometary nuclei and large-particle clouds

Since a coma is nearly transparent at. radio wavelengths, radar is better equipped to inspect a cometary nucleus than are optical and infrared methods (e.g., Kamoun et al., 1982), and radar observations of several comets (Table I) have provided some useful constraints on nuclear dimensions, spin vectors, and surface morphologies. The most informative experiment to date, of IRAS-Araki-Alcock, which came within 0.03 AU of Earth in 1983 (Fig. 4), yielded echoes with a narrowband component from the nucleus as well as a much weaker broadband component attributed to large particles ejected mostly from the sunlit side of the nucleus (Harmon et al., 1989) . The particles are probably several centimeters in size and appear to be distributed within -1000 km of the nucleus, i.e., in the volume filled by particles ejected at several meters per second over a few days. Radar observations of comet Halley (Campbell et al. 1989) yielded echoes with a substantial broadband component but. no component_ as narrowband as that expected from the nucleus, whose dimensions and spin vector were constrained by Giotto and Vega images. 'l'he echo's bandwidth and radar cross section suggest that it arises predominantly from coma particles with radii > 2 cm. Hence at least two very different comets have been accompanied by swarms of large particles. There are obvious implications for spacecraft encounters with comets, including the extreme case of terminal interception.

IV. Scenarios FOR RADAR Reconnaissance OF Potential NEO HAZARDS

The Immediate Future

Arecibo and Goldstone have been the primary NEO radar observatories during the past decade. This situation is unlikely to change during the next decade, notwithstanding prospects for occasional G-VLA and V-E bistatic observations of NEOS that make very close approaches with lead times of at least several months. Similarly, efforts to convert existing military radars to other applications may result in detection of some NEOs by those instruments, but it is unlikely that the results of such endeavors will be very competitive with Arecibo/Goldstone experiments in the near future.

Table III lists the radar-astrometric range limits expected for Arecibo and Goldstone by 1995, when the hardware upgrades mentioned earlier should be completed. Most of the optically discoverable Earth-crossers traverse the joint Arecibo-Goldstone detectability window at least once every few decades. Arecibo, with nearly 40 times the sensitivity of Goldstone, will see twice as far and cover three times as much volume as Goldstone, and hence will be the key instrument for NEO radar reconnaissance. Goldstone, with a solid angle window twice the size of Arecibo's and an hour-angle window at least several times wider than Arecibo's for any given target, will serve a complementary role, especially for newly discovered objects.

Discovery apparition geometry often is exceptionally favorable to radar reconnaissance. For this reason, and in view of the utility of radar observations for orbit refinement and physical characterization, there is compelling motivation to do radar observations of newly discovered Earth-crossers whenever possible. However, NEOS pass through each instrument's radar detectability window very rapidly and the timing of an object's discovery relative to its passage through the Arecibo and Goldstone windows is unpredictable. Figure 5 plots SNRS that could have been attained by the upgraded (post–1994) Arecibo and Goldstone telescopes between June 1990 and June 1991 for NEAs discovered during that period. As illustrated by that figure, it is common for Earth-approachers tobe discovered after they have left one or both of the two radar windows. One of Goldstone's jobs will be to follow-up discoveries that Arecibo cannot.. Similarly, many new NEOs pass through both windows after discovery, but during intervals separated by days or

weeks. In such situations, even if Arecibo observations are possible, Goldstone can greatly extend the orbital coverage of the radar observations, thereby lengthening the astrometric arc and improving the orbit estimation. Furthermore, depending on the target's echo strength during the "first" instrument's observations and the quality of the optical astrometry used to make the initial radar ephemeris, measurements with high-resolution waveforms may not be possible before the target leaves the first instrument's window. In this case the second instrument- would inherit an improved delay-Doppler ephemeris that would permit quick progression to high–resolution waveforms, extension of the astrometric arc, and efficient determination of physical properties. Experiences with 1989 JA, 1989 PB, 1990 MF, 1991 JX, and Toutatis were like this.

Given the capabilities of existing radars, how much of the potential follow-up work on NEOS will actually be done? Minimal reconnaissance of a new NEO will require at least one block of time, probably at least two hours long, on one of a handful of possible dates, to be scheduled with extremely short notice (typically on the order of a few days to a few weeks) . During 1989-1993, 11 new NEOS were observed (seven were detected) at Arecibo and/or Goldstone under such circumstances, causing difficult scheduling adjustments. By 2000, the upgraded Arecibo might have nearly monthly opportunities to make thousand-pixel images of an ECA during a post-discovery apparition and weekly opportunities to do orbit-securing astrometry on a new object (Table IV) . Imaging with enough coverage of subradar longitude and/or latitude to allow high-precision reconstruction of shape and spin vector probably would require at least, one or two full tracks, i.e., much more than just an "astrometric" detection. It will not be easy for Arecibo to establish policy for dealing with an onslaught of target-of-opportunity situations. NAIC, a national center operated primarily for visitors engaged in passive radio astronomy and ionospheric physics, operates around the clock daily and is still oversubscribed. (About 4% of the Lime has been used for planetary radar.) The pressure on the schedule after the upgrade will be severe. It seems prudent to assume that it may not be possible for Arecibo to look at more than a few tens of percent of the new NEOs that it could see. While some fraction of new NEO radar opportunities will be observable with GoldsLone and perhaps the E-B system, the pressure on DSN tracking allocations from flight

projects is severe and is increasing, and the logistical impediments to short-notice E-B observations *are* daunting.

The Post-Spaceguard Era

If the proposed Spaceguard Survey comes to pass, the catalog of known NEAs will swell to over 100 times its current size. Soon after the Survey gets started, the frequency with which known ECAS traverse the radar windows will dwarf that in the Fig. 5 simulation. Less than half way through the survey there will be several times as many cataloged ECAS as there are numbered mainbelt asteroids today. The initial orbits of newly discovered objects will be inaccurate, and the volume of follow-up work needed to secure orbits will rapidly become enormous. Reliable extrapolation of orbits will not be possible until the astrometric database matures to a certain point, either through protracted optical follow-up over a long time span or with radar measurement.s over a very much shorter time span. The appeal of using radar for orbit refinement will grow in proportion to the number of predicted close approaches of new objects, because of the anxiety instilled by the uncertainties in the extrapolated orbits. Moreover, although sub-100-m objects are far below the threshold for global climatic effects, people may not find that. qualification very comforting if we are totally unable to predict the impact parameter for an object on an extremely close-approach trajectory. Of course, predictions of very close approaches by large asteroids will be taken seriously.

Consider the inevitable discovery of objects that threaten to come very close, e.g., within one lunar distance, keeping in mind the fact that the frequency of cislunar misses is -3600 times higher than the collision frequency. For example, consider 10,000-MT objects, -500 m in diameter, which are at the small. end of the range of estimates for the local/global transition. Collisions with such objects are 63,000 y apart on average, so cislunar misses are 18 y apart. Spaceguard will discover --640(1 of those objects, i.e., ~70% of the -9200 in the population. One of those 6400 objects will make a cislunar miss every -25 years. However, uncertainties in orbital extrapolations much more than a century into the future may not permit confident distinction of close-call trajectories from impact trajectories, at least until the astrometric time base is many decades long. Of course, this example could have considered the flux of objects within 10 lunar distances, or whatever; the important. quantity is the impact parameter in units of its uncertainty

Society will surely want to reduce uncertainties associated with predictions of extremely close approaches of NEOs, and radar is the most efficient groundbased technique for trajectory refinement. However, existing instrumentation will hardly be able to do follow-up observations of the bulk of ECAs discovered with Spaceguard. That task would require instrumentation dedicated to this work, at least as sensitive as the upgraded Arecibo, and able to see most of the sky. TWO fully steerable radars, one each in the northern and southern hemispheres, designed specifically for NEO reconnaissance, would satisfy these requi.rements. (None of the active instruments were optimized for planetary radar astronomy.) With current Technology, it 'might be possible to build a steerable telescope ten times more sensitive than the upgraded Arecibo for as little as 100 M$. For $lB, it would be possible, even with 20th century technology, to build six globally distributed, each an order of magnitude more sensitive than the upgraded Arecibo. The radar and Spaceguard optical nets would be linked and highly automated, so radar could acquire new objects right after they were found. Radar sequences and ephemeris refinement would be run by an intelligent program that could progress from initial detection to imaging within minutes. Six telescopes could respond to -100 new objects daily. Follow-up would be extremely efficient and would suffice to identify any close approaches during the next century. In terms of information gained, each radar telescope would be considerable cheaper than spacecraft flybys.

Once Spaceguard begins, there will be an outstanding imaging opportunity every month or so (Table IV) . By then, the sophistication of inversion methods may allow delay-Doppler images to be piped in real time to software that will return a "running reconstruction" of the target's shape and rotational orientation. In principle, an IAU telegram consisting of an animation file showing the 3-D model, properly orientated as a function of UTC, could be circulated globally within days of discovery.

The Next Millennium

At any time in the future, the role of groundbased radar in response to the NEO hazard will depend on the state of technology and the nature of civilization, neither of which can be confidently foreseen more than a few decades hence. If civilization endures through the next millennium, our descendants may decide to maintain a groundbased, small-body radar reconnaissance system indefinitely as insurance against hazards from long-

period comets. Note that the risk of a civilization-ending impact during the next century is about the same as the risk of a civilization-ending LPC impact during the next millennium. Also note that whereas the warning time for an asteroid (in the post-Spaceguard era) is likely to be at least a century and hence more than adequate for mitigation at a comfortable pace, the warning time for an LPC would probably be less than one year. Moreover, LPC trajectory extrapolation will be hampered by obscuration of the nucleus and by uncertainties about nongravitational forces. Several cislunar misses by LPCs can be expected during the next millennium. The uncertainty in trajectory extrapolation after discovery of these objects could be terrifying, and any number of panic scenarios are possible. Needless to say, radar astrometry would be precious under such circumstances.

Acknowledgment . This research was conducted at the Jet Propulsion Laboratory," California Institute of Technology, under contract with the National Aeronautics and Space Administration (NASA).

REFERENCES

Campbell, D. B., Harmon, J. K., Hine, A. A., Shapiro, I. I., Marsden, B. G.,and Pettengill, G. H. 1983. Radar observations of comets IRAS-Araki-Alcock and Sugano-Saigusa-Fujikawa *Bull . Am. Astron. Sot.* 15:800 (abstract).

Campbell, D. B., Harmon, J. K., and Shapiro, I. I. 1989. Radar observations of comet Halley. *Astrophys J.* 338:1094-1105.

Campbell, D. B., Pettengill, G. H., and Shapiro, I. I. 1976. 70-cm radar observations of 433 Eros. *Icarus 28: 17-20.*

de Pater, 1., Palmer, P., Snyder, I,. E., Ostro, S. J., Yeomans, D. K., and Mitchell, D. L. 1992. Bistatic radar observations of asteroids 324 Bamberga, 7 Iris, and 1991 EE. *Bull. Amer.* Astron. Sot. 24:934 (abstract.)

de Pater, 1., Palmer, P., Snyder, I,. E., Ostro, S. J., Yeomans, D. K., and Mitchell, D. L. 1993. Bistatic radar and passive microwave observations of asteroids. In preparation.

Goldstein, R. M. 1969a. Radar observations of Icarus, *Icarus* 10: *430-431.*

Goldstein, R. M. 1969b. Radar observations of Icarus. *Science* 162: 903-904.

Goldstein, R. M., Holdridge, D. B., and Lieske, J. H. 1973. Minor planets and related objects. XII. Radar observations of 1685 Toro. *Astron. J.* 78:508-509.

Goldstein, R. M., Jurgens, R. F., and Yeomans, D. K. 1981. Radar observations of Apollo. *Icarus 48: 59-61.*

Goldstein, R. M., Jurgens, R. F., and Sekanina, Z. 1984. A radar study of comet IRAS-Araki-Alcock 1983d. *Astron. J.* 89:1745-1754.

Harmon, J. K., priv. comm.

Harmon, J. K., D. B. Campbell, A. A. Hine, I. I. Shapiro, and B. G. Marsden 1989. Radar observations of comet IRAS-Araki-Alcock 1983d. *Astroph. J.* 338:1071-1093.

Hudson, R. S., 1992. Three-dimensional. shapes of near-earth objects from radar. *Eos* Trans. AGU 73, AGU *1992 Fall Mtg. Abstract Supp., 335.*

Hudson, R. S., 1993. Three-dimensional reconstruction of asteroids from radar observations , *Remote Sensing Reviews* (in press).

Hudson, R. S., and Ostro, S. J. 1990. Doppler radar imaging of spherical planetary surfaces. *J. Geophys. Res.* 95:10947-10963.

Hudson, R. S., and Ostro, S. J. 1993. Reconstruction of the shape of asteroid 4769 Castalia from inversion of radar images. In preparation.

Jurgens, R. F., and Goldstein, R. M. 1976. Radar observations at 3.5 and 12.6 cm wavelength of asteroid 433 Eros. Icarus 28: 1-15.

Kamoun, P. G., Campbell, D. B., Ostro, S. J., Pettengill, G. H., and Shapiro, I. I. 1982. Comet Encke: Radar detection of nucleus. *Science* 216:293-296.

Kamoun, P. G. 1983. Radar Observations of Cometary Nuclei. Ph.D. thesis, MIT .

Melosh, H. J., and Stansberry, J. A. 1991. Doublet craters and the tidal disruption of binary asteroids. *Icarus* 94:171-179.

Mishchenko, M. I., 1992. Polarization characteristics of the coherent backscatter opposition effect. *Earth, Moon, Planets* 58:127-144.

Morrison, D (cd.) 1992. The Spaceguard Survey: Report of the NASA International Near-Earth-Object Detection Workshop.

Ostro, S. J., Campbell, D. B., and Shapiro, I. I. 1983. Radar observations of asteroid 1685 Toro. *Astron. J.* 88:565-576.

Ostro, S. J., Harris, A. W., Campbell, D. B., Shapiro, I. I., and Young, J. W. 1984. Radar and photoelectric observations of asteroid '2100 Ra-Shalom. *Icarus* 60:391-403.

Ostro, S. J., Campbell, D. B., and Shapiro, I. I. 1985. Mainbelt asteroids: Dual-polarization radar observations. Science 224:442-446.

Ostro, S. J., Yeomans, D. K., Chodas, P. W., Goldstein, R. M., Jurgens, R. F., and Thompson, T. W. 1986. Radar observations of asteroid 1986 JK. *Icarus* 78:382-394.

Ostro, S. J., Connelly, R., and Belkora, L. 1988. Asteroid shapes from radar echo spectra: A new theoretical approach. *Icarus* 73: 15-24.

Ostro, S. J., Campbell, D. B., Hine, A. A., Shapiro, I. I., Chandler, J. F., Werner, C. L., and Rosema, K. D. 1990. Radar images of asteroid 1627 Ivar. *Astron. J.* 99:2012-2018.

Ostro, S. J., Chandler, J. F., Hine, A. A., Shapiro, I. I., Rosema, K. D., and Yeomans, D. K. *1990.* Radar images of asteroid 1989 PB. *Science* 248:1523-1528.

Ostro, S. J., Campbell, D. B., Chandler, J. F., Hine, A. A., Hudson, R, .S., Rosema, K. D., and Shapiro, I. I. 1991a, "Asteroid 1986 DA: Radar evidence for a metallic composition. *Science* 252:1399-1404.

Ostro, S. J., Campbell, D. B., Chandler, J. F., Shapiro, I. I., Hine, A. A., Velez, R., Jurgens, R. F., Rosema, K. D., Winkler, R., and Yeomans, D. K. 1991b. Asteroid radar astrometry. *Astron. J.* 102:1490-1502.

Ostro, S. J., Harmon, J. K., Hine, A. A., Perillat, P., Campbell, D. B., Chandler, J. F., Shapiro, I. I., Jurgens, R. F., and Yeomans, D. K. 1991c. Bull. Amer. *Astron. Sot.* 23:1144 (abstract).

Ostro, S. J.,Jurgens, R. F., Rosema, K. D., Winkler, R., Howard, D., Rose, R., Slade, M. A., Yeomans, D. K., Campbell, D. B., Perillat p., Chandler, J. F., Shapiro, 1.1., Hudson R. S., Palmer, P., and de Pater, I. 1993. Radar imaging of asteroid 4179 Toutatis. *Bull. Am. Astron. Soc. 25,* in press (abstract) .

Pettengill, G. H., Shapiro, 1. I., Ash, M. E., Ingalls, R, P., Rainville, L. P., Smith, W. B., and Stone, M. L. 1969. Radar observations of Icarus. *Icarus* 10:432-435.

Pettengill, G. H., Ostro, S. J., Shapiro, I. I., Marsden, B. G., and Campbell, D. B. 1979. Radar observations of asteroid 1580 Betulia. Icarus 40:350-354.

Sagan, C., and Ostro, S. J. 1993. Long-range human consequences of interplanetary collision hazards. In preparation.

Seidelmann, P. K., B. Guinot, and L. E. Doggett, 1992. Time. In Explanatory *Supplement to the Astronomical Almanac,* ed. P. K. Seidelmann (Mill Valley, CA: University Science Books), PP. 39-93.

Shoemaker, E. M., Wolfe, R. F. and Shoemaker, C. S. 1990. Asteroid and comet flux in the neighborhood of the Earth. In *Global. Catastrophes in Earth History; An Interdisciplinary Conference on Impacts, Volcanism and Mass* Mortality (Geol. Sot. of America Special Paper 247, Boulder) pp. 155-170.

Standish, E. M., Newhall, X X, Williams, J. G., and Yeomans, D.K. 1992. Orbital ephemerides of the sun, moon, and planets. In *Explanatory Supplement to the Astronomical Almanac,* ed. P. K. Seidelmann (Mill Valley, CA: University Science Books), PP. 279-323.

Stacy, N. J. S. 1983. High-Resolution Synthetic Aperture Radar Observations of the Moon. Ph.D. thesis, Cornell University.

Yeomans, D. K., Ostro, S. J., and Chodas, P. W. 1987. Radar astrometry of near-Earth asteroids. *Astron. J. 94: 189-200.*

yeomans, D. K., Chodas, P. W., Keesey, M. S., Ostro, S.J., Chandler, J.F., and Shapiro, I. I. 1992. Asteroid and comet orbits using radar data. *Astron. J.* 103:303-317.

Zaytsev, A. L., Sokolsky, A. G., Wielebinski, R., Vyshlov, A. S., Grishmanovsky, V. A., Altenhoff, W. J., Rzhiga, O. N., Shor, V. A., Koluka, Yu. F., Shubin, V. A., Krivtsov, A. P., Zaytseva, O. S., Margorin, O. K., and Nabatov A. S. 1993. 6-cm Radar observation of (4179) Toutatis. *Asteroids Comets Meteors 1993 Abstract Book,* in press (abstract) .

TABLE I[a]

Year	Target	Reference (Site, λ cm)
1.968	1566 Icarus	1 (G, λ13); 2 (H, λ3.8)
1972	1685 Toro	3 (G, λ13)
1975	433 Eros	4 (G, λ3.5, λ13); 5 (A, λ70)
1976	1580 Betulia	6 (A, λ13)
1980	1685 Toro[b]	7 (A, λ13)
	1862 Apollo	8 (A, λ13); 9 (G, λ3.5)
	comet Encke	10 (A, λ13)
1981	1915 Quetzalcoatl	8 (A, λ13)
	2100 Ra-Shalom	11 (A, λ13)
1.982	comet Grigg-Skjellerup	12 (A, λ13)
1983	1620 Geographos	8 (A, λ13)
	comet IRAS-Araki-Alcock	13 (A, λ13); 1.4(G, λ3.5)
	2201 Oljato	8 (A, λ13)
	comet Sugano-Saigusa-Fujikawa	15,16 (A, λ13)
1984	2101 Adonis	8 (A, λ13)
	2100 Ra-Shalom[b]	8 (A, 2.13)
1985	1627 Ivar	17 (A, λ13)
	1036 Ganymed	8 (A, λ13)
	comet Halley	18 (A, λ 13)
	1866 Sisyphus	8 (A, λ13)
1986	1986 DA	19 (A, λ13)
	1986 JK	20 (G, λ3.5)
	3103 (1982 BB)	8 (A, λ13)
	3199 Nefertiti	8 (A, λ13)
1987	1981 Midas	8 (G, λ3.5)
	3757 (1982 XB)	8 (A, λ13)
1988	1685 Toro[c]	8 (A, λ13)
	3908 (1980 PA)	8 (A, λ13; G, λ3.5)
	433 Eros[b]	8 (A, λ13)
1989	4034 (1986 PA)	8 (A, λ13)
	1580 Betulia[b]	8 (G, λ3.5; A, λ13)
	1989 JA	8 (A, λ13; G, λ3.5)
	4769 Castalia	21 (A, λ13; G, λ3.5)
	1917 Cuyo	8 (A, 2.13; G, λ3.5)
1990	1990 MF	8 (A, λ13; G, λ3.5)
	1990 0s	8 (G, λ3.5)
	4544 Xanthus	8 (A, λ13)
1991	1991 AQ	22 (A, λ13)
	1991 JX	22 (A, λ13; G, λ3.5)
	3103 (1982 BB)[b]	23 (G, λ3.5)
	1991 EE	23 (A, λ13); 24 (GV, λ3.5)
1992	1981 Midas[b]	2.3 (G, λ3.5)
	5189 (1990 UQ)	23 (G, λ3.5)
	4179 Toutatis	25 (A, λ13; G, λ3.5); 26(YE, λ6); 27 (GV, λ3.5)

[a]Site abbreviations correspond to Goldstone, Haystack, Arecibo, Goldstone-VLA, and Yevpatoria-Effelsberg. Observations are listed and cited chronologically. References: 1: Goldstein (1969a,b); 2: Pettengill et al. (1969); 3: Goldstein et. al. (1973); 4: Jurgens and Goldstein (1976); 5: Campbell et al. (1976); 6: Pettengill et al. (1979); 7: Ostro et al. (1983); 8: Ostro et al. (1991b); 9: Goldstein et al. (1981); 10: Kamoun et. al. (1982); 11: Ostro et al. (1984); 12: Kamoun (1983); 13: Harmon et al. (1989); 14: Goldstein et al. (1984); 15: Campbell et al. (1983); 16: Harmon priv. comm; 17: Ostro et al.. (1990); 18: Campbell et al. (1989); 19: Ostro et al. (1991a); 20: Ostro et al. (1989); 21: Ostro et al. (1990); 22: Ostro et al. (1991c); 23: Ostro et al., unpublished; 24: de Pater et al. (1992); 24: Ostro et al. (1993); 26: Zaytsev et al. (1993); 27: de Pater et al. (1993).

[b]second apparition yielding radar detection.

[c]third apparition yielding radar detection.

Table II. Effect of delay/Doppler measurements on extrapolation of 1991 JX'S orbit from discovery-apparition astrometry. Uncertainties in the asteroid's April 2019 position, predicted from 54 optical measurements obtained from May 9 to July 3, are given in the top row. The bottom row gives uncertainties for a prediction that includes 24 delay-Doppler measurements from June 5-15. (D. K. Yeomans, priv. comm.)

Dataset	Positional Uncertainty		
	kilometers	Earth radii	lunar distances
Optical	8,000,000	1260	21
Optical + Radar	25,000	4	0.07

TABLE III. Range limits (AU) for radar astrometry of new NEOs. These limits correspond to a single-date SNR of 20 and telescope sensitivities expected by 1995, i.e., upon completion of upgrades begun in the early 1990s.

Diameter	Arecibo	Goldstone
10 m	0.043	0.016
100 m	0.10	0.041
1 km	0.24	0.10
10 km	0.59	0.24

Table IV. Mean intervals between ECA approaches close enough to yield three different values of single-date SNRS with the upgraded Arecibo telescope. Calculation of distances (R) for each SNR and asteroid diameter assumed nominal asteroid properties. The intervals were scaled from values taken by eye from Fig. 2 of Shoemaker (1990).

Early 1990s

	SNR = 10,000		SNR = 1,000		SNR = 100		SNR = 20	
D (km)	R (AU)	int'l	R (AU)	int'l	R (AU)	int'l	R (AU)	int'l
3	0.078	45 y	0.14	10 mon	0.24	4 mon	0.37	2 mon
1	0.052	2 y	0.092	5 mon	0.16	7 wk	0.25	20 d
0.3	0.033	8 y	0.059	2 y	0.1	7 mon	0.16	3 mon
0.1	0.022	25 y	0.038	8 y	0.067	2 y	0.10	1 y

After Spaceguard

	SNR = 10,000		SNR = 1,0.00		SNR = 100		SNR = 20	
D (km)	R (Au)	int'l	R (AU)	int'l	R (AU)	int'l	R (AU)	int'l
3	0.078	10 y	0.14	2 mon	0.24	3 wk	0.37	10 d
1	0.052	2 mon	0.092	2 wk	0.16	1 wk	0.25	2"d
0.3	0.033	1 mon	0.059	1 wk	0.1	2 d	0.16	I d
0.1	0.022	1 mon	0.038	2 wk	0.067	3 d	0.10	I d

Figure CAPTIONS

1. Radar system sensitivities. The single-date SNR of echoes from a "typical" l-km asteroid at a distance of 0.1 AU is plotted against declination for Goldstone (G), the Goldstone-VLA system (G-VLA), Arecibo (A), and the upgraded Arecibo (A_{up}) .

2. Radar reduction of instantaneous range-prediction error for selected asteroids, vs. days since the initial radar detection of the object (or, for 1685 Toro, since the first detection during the 1988 apparition) at Goldstone (dotted curves) or Arecibo (all other curves). All objects are Earth-crossers except mainbelt asteroid 105 Artemis. Two-letter abbreviations correspond to 1986 DA, 1989 PB, 1990 MF, 1991 AQ, and 1991 JX. For 1990 MF and 1991 JX, Arecibo astrometry was used in making ephemerides for Goldstone observations, which began eight days and three days, respectively, after the last Arecibo observation.

3. 13-cm radar properties for near-Earth asteroids 1986 DA, 3199 Nefertiti, 1620 Geographos, 1980 PA, 1685 Toro, 1627 Ivar, 4769 Castalia, and 2101 Adonis (whose albedo is uncertain), compared to those for other planetary targets. Symbols are used for the Moon, Venus, and Mars; the circled numbers denote mainbelt asteroids 1 Ceres, 4 Vesta, and 16 Psyche; and rectangles identify the Galilean satellites Io, Europa, Ganymede, and Callisto.

4. Arecibo OC and SC echo spectra obtained for Comet IRAS-Araki-Alcock, truncated at 2% of the maximum OC amplitude. The narrowband echo from the nucleus is flanked by broadband echo from large particles in a cloud surrounding the nucleus. (Harmon et al., 1989.)

5. Single-date SNRS during June 1990 to June 1991 for ECAS discovered during that period, with upgraded (post-1994) capabilities assumed for Arecibo (solid. curves) and Goldstone (dashed curves) . The horizontal position of the dot on the border around each asteroid designation indicates the discovery date. Seven asteroids discovered during this 13-month period would not. have been observable then.

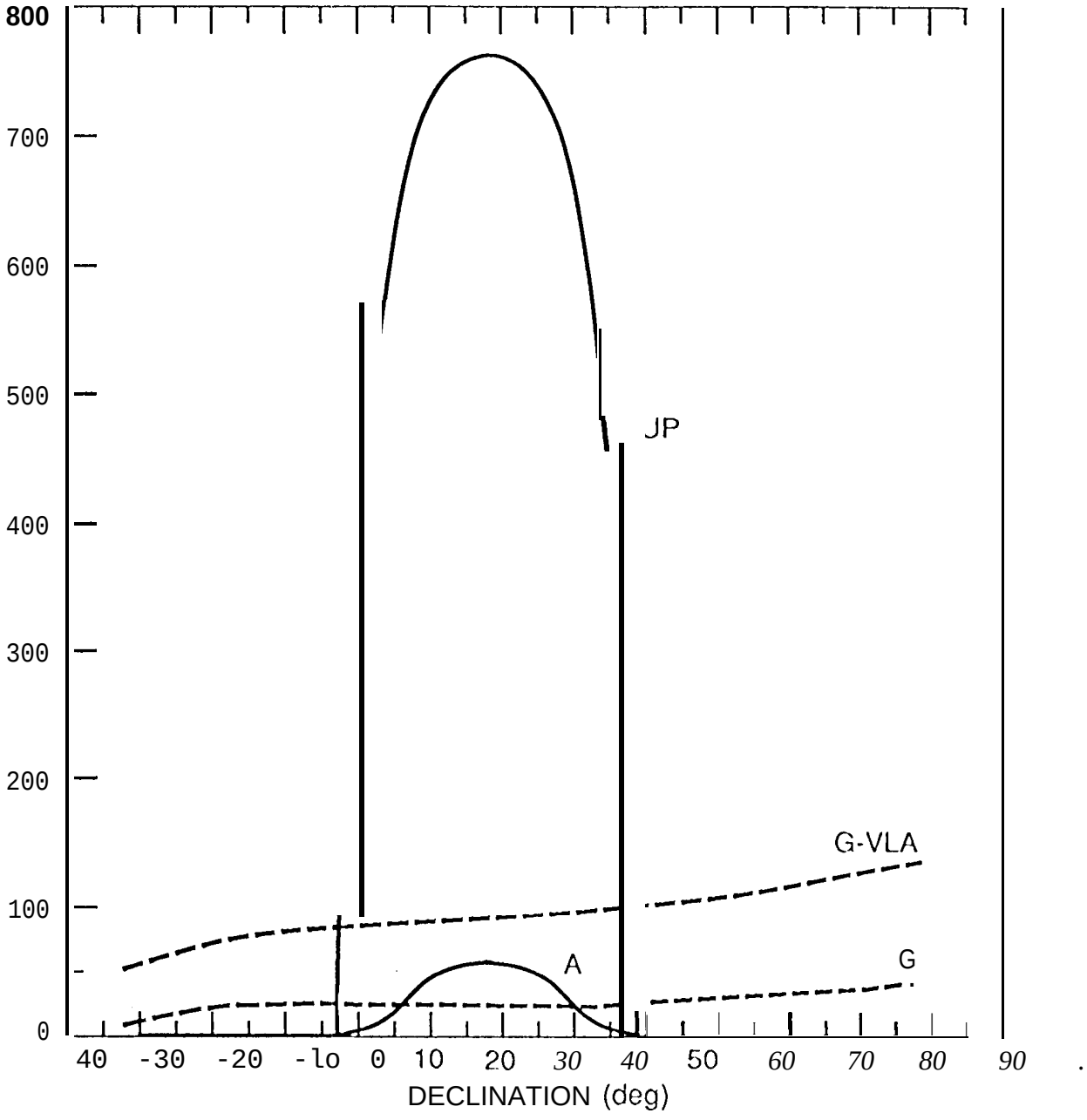
800
700
600
500
400
300
200
100
0
JP
G-VLA
A
G
40 -30 -20 -lo 0 10 20 30 40 50 60 70 80 90
DECLINATION (deg)

Ostro Fig. 1

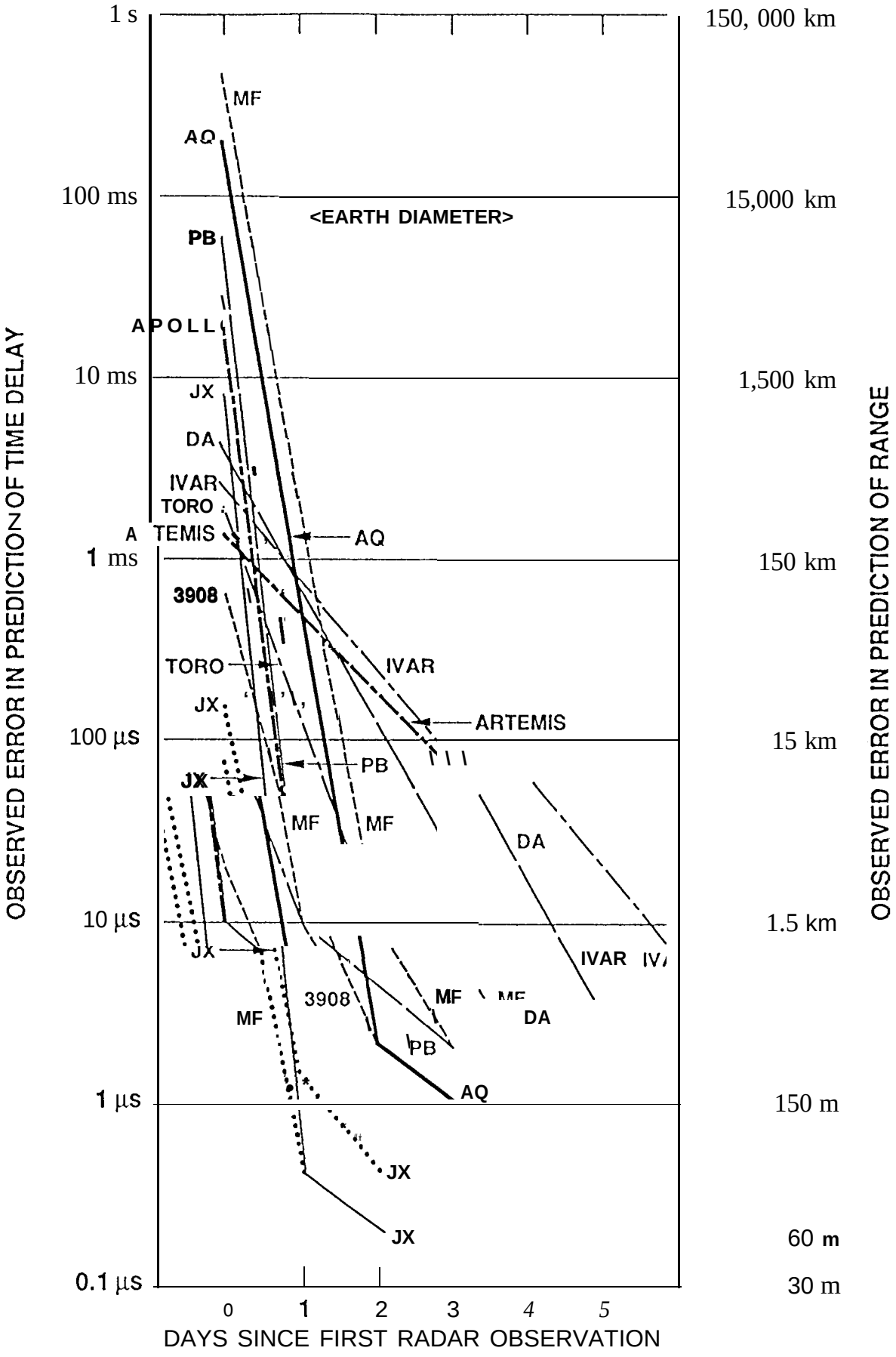
1 s
100 ms
10 ms
1 ms
100 μs
10 μs
1 μs
0.1 μs
150, 000 km
15,000 km
1,500 km
150 km
15 km
1.5 km
150 m
60 m
30 m
<EARTH DIAMETER>
MF
AQ
PB
APOLLO
JX
DA
IVAR
TORO
ARTEMIS
TEMIS
3908
ARTEMIS
0
1
2
3
4
5
OBSERVED ERROR IN PREDICTION OF TIME DELAY
OBSERVED ERROR IN PREDICTION OF RANGE
DAYS SINCE FIRST RADAR OBSERVATION

Ostro Fig. 2

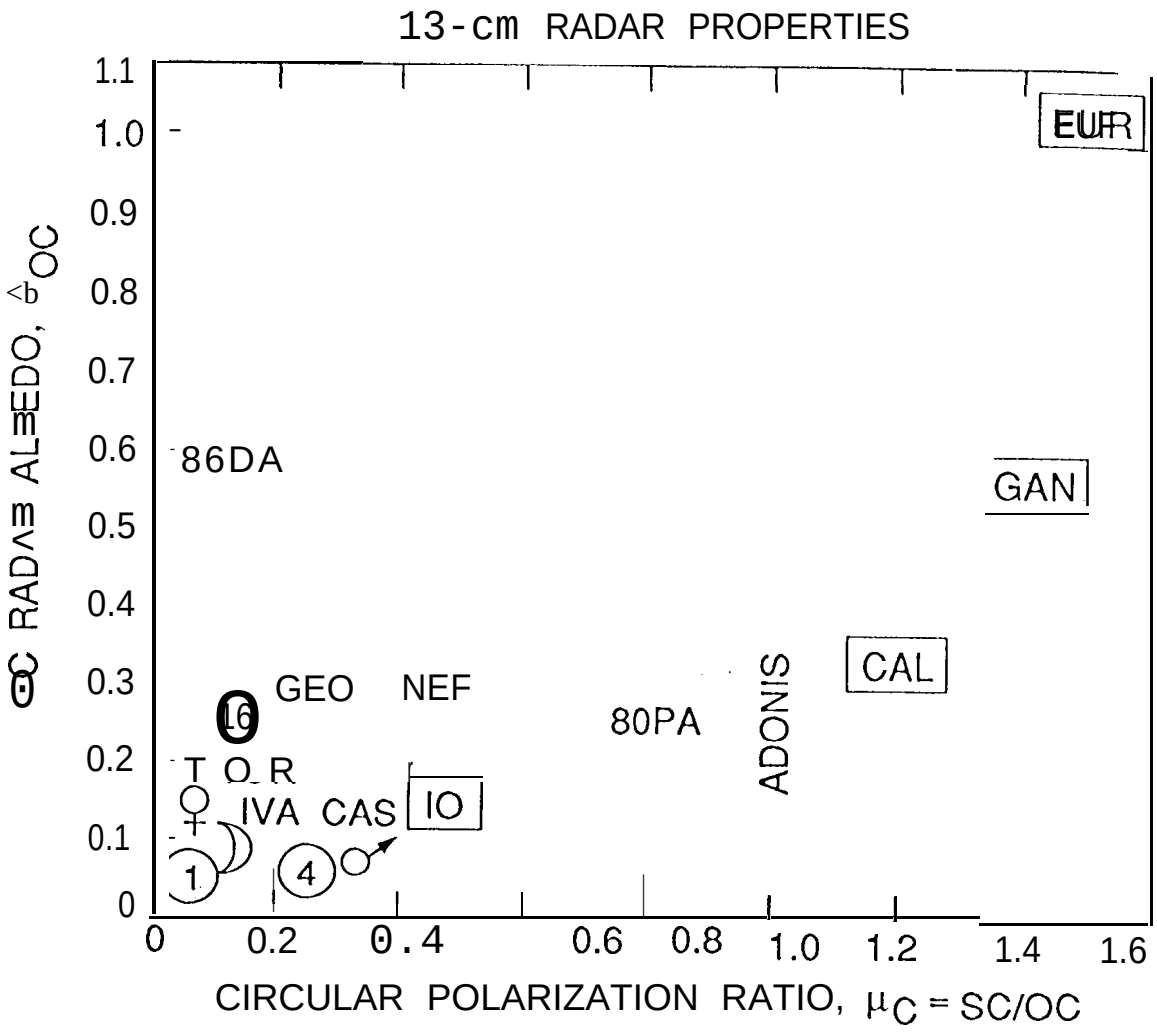
13-cm RADAR PROPERTIES
1.1
1.0
0.9
0.8
0.7
0.6
0.5
0.4
0.3
0.2
0.1
0
0
0.2
0.4
0.6
0.8
1.0
1.2
1.4
1.6
EUR
GAN
CAL
IO
86DA
GEO
NEF
80PA
ADONIS
IVA
CAS
1
4
CIRCULAR POLARIZATION RATIO, μC = SC/OC

Ostro Fig. 3

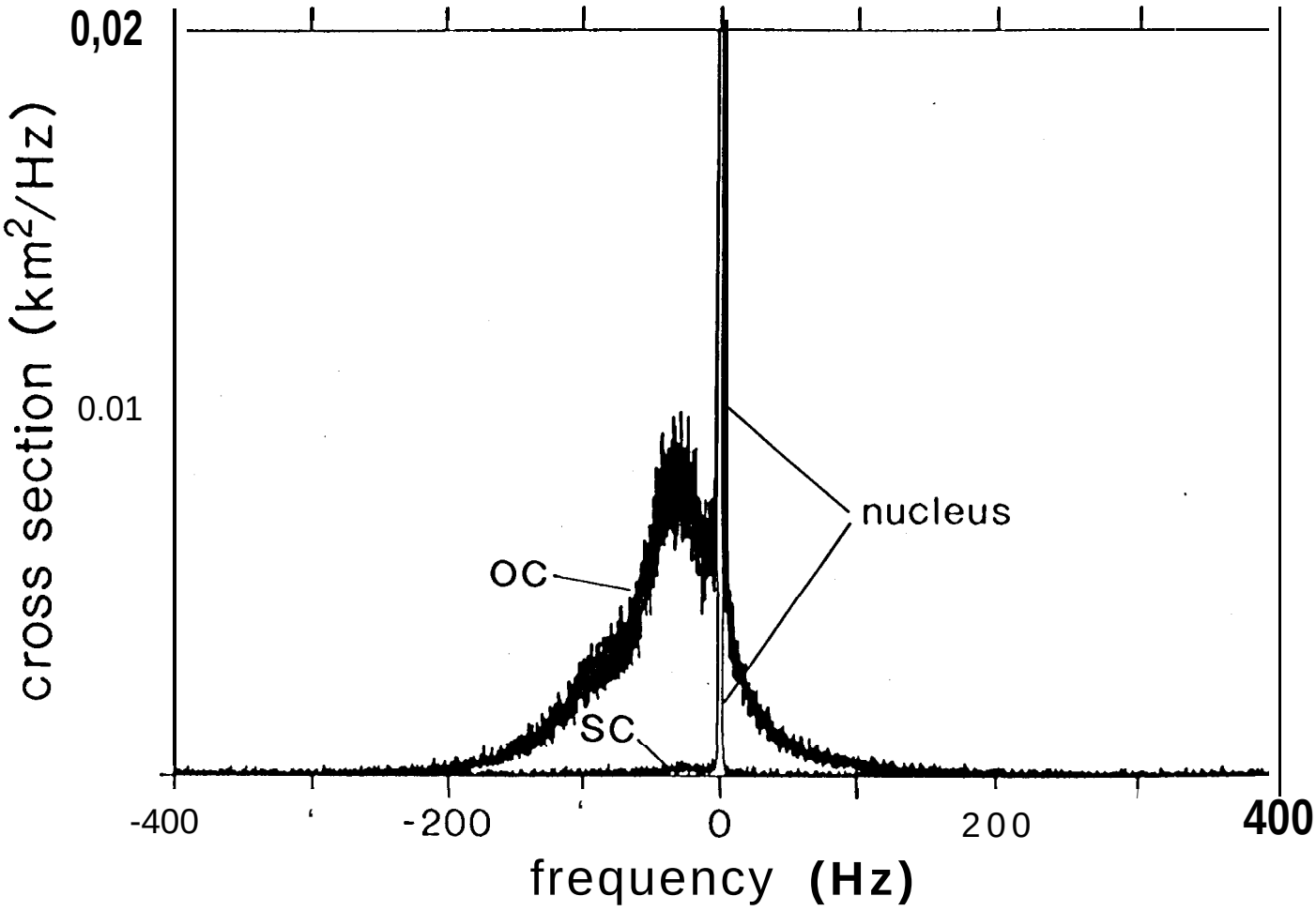
0,02
0.01
cross section (km²/Hz)
nucleus
OC
SC
-400
-200
0
200
400
frequency (Hz)

Ostro Fig. 4

Radar Investigation of New NEAs during 6/90 - 6/91, with Upgraded Capabilities Assumed for Arecibo and Goldstone

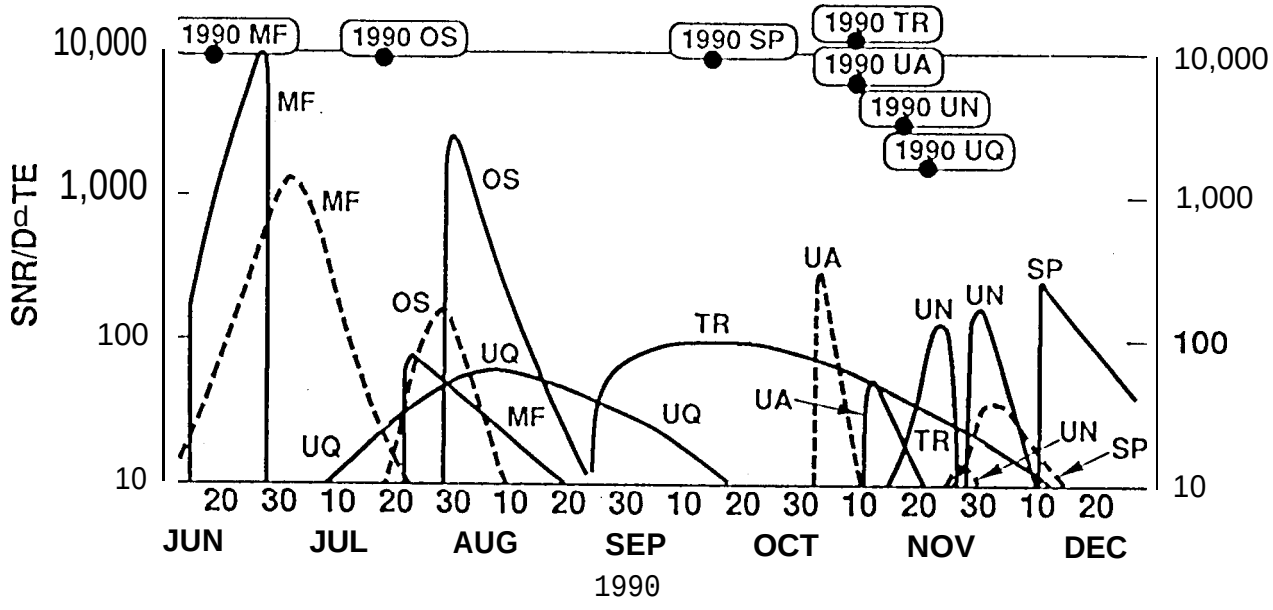

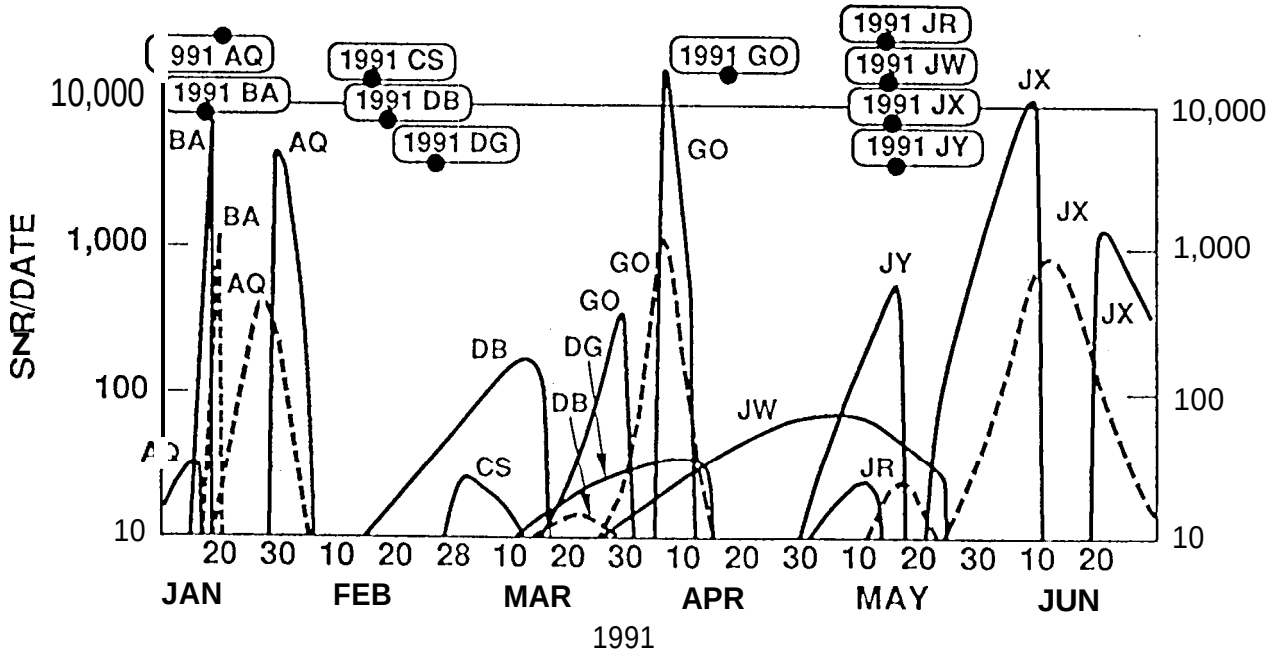

Ostro Fig. 5